



**Subject Areas:**

Fluid mechanics, geophysics, wave motion

**Keywords:**

Westward drift, Rossby waves, quasi-geostrophy, Earth's outer core

**Author for correspondence:**

O. P. Bardsley [e-mail: ob275@cam.ac.uk](mailto:ob275@cam.ac.uk)

# Could hydrodynamic Rossby waves explain the westward drift?

O. P. Bardsley<sup>1</sup>

<sup>1</sup>Department of Engineering, University of Cambridge, Trumpington Street, Cambridge, CB2 1PZ

A novel theory for the origin of the westward drift of the Earth's magnetic field is proposed, based upon the propagation of hydrodynamic Rossby waves in the liquid outer core. These waves have the obscure property that their crests always progress eastwards — but for a certain subset, energy can nevertheless be transmitted westwards. In fact, this subset corresponds to sheet-like flow structures, extended in both the axial and radial directions, which are likely to be preferentially excited by convective upwellings in the Earth's rapidly-rotating outer core. To enable their analysis, the *quasi-geostrophic* approximation is employed, which assumes horizontal motions to be independent of distance along the rotation axis, yet accounts for variations in the container height (i.e. the slope of the core-mantle boundary). By projecting the momentum equation onto flows of a quasi-geostrophic form, a general equation governing their evolution is derived, which is then adapted for the treatment of two initial value problems — in both Cartesian and spherical geometries — which demonstrate the preference for westward energy propagation by the waves in question. The merits of this mechanism as an explanation for westward drift are discussed.

## 1. Introduction

Since its discovery over three centuries ago by Halley [1], the westward drift of the Earth's magnetic field has remained an intriguing problem in geophysics. Why should it be that many features of the observable geomagnetic field have systematically tracked west throughout 400 years of measurements? The first detailed analysis of this phenomenon was performed by Bullard *et al.* [2], to be followed by many others (see [3]) seeking to elucidate its behaviour through interrogation of both historical data and recent satellite measurements.

The allure of westward drift can perhaps be put down to its ubiquity. Regardless of whether one looks at maps of declination at the Earth's surface or radial field at the core-mantle boundary, westward drift arises as a robust feature of geomagnetic secular variation. The apparent indifference to both spatial scale [4] and epoch [5] suggests that the westward drift is an artefact of fundamental core dynamics, and therefore its explanation may open a window onto the Earth's deep interior.

Whilst the westward drift spans many temporal and spatial scales, it also appears to be geographically localised, with secular variation being limited to low-latitude (equatorial) regions [5–7], and dominated by the motion of intense flux spots with a tendency to pair north and south of the equator [8]. For unknown reasons, the Pacific hemisphere appears to have been relatively quiet in the modern era [9], with a weaker field magnitude and lack of any convincing secular variation patterns. The dominant contribution to westward drift – centred over the equator in the Atlantic hemisphere – was found by Finlay and Jackson [5] to be at a rate of  $0.27^\circ$  per year, or 17km per year at the core-mantle boundary. It is worth noting, however, that these observations face an unfortunate constraint; owing to the interference of crustal magnetism, their resolution is limited to spherical harmonic degrees below 13 — meaning there is a dearth of information at all but the largest scales of magnetic field [10]. This is a cause for concern, especially since spectra of the observable secular variation show its power increasing with harmonic degree [4], suggesting its origin is to be found at the invisible small scales. Therefore, theoretical models of the small-scale dynamics may prove useful tools for explaining the westward drift.

The liquid outer core, approximately occupying the spherical shell 1,231–3,485km from the Earth's centre, is the cradle of our planet's magnetic field. Its periphery – the core-mantle boundary – may be considered an impermeable, electrically insulating solid on the timescales of interest. Its internal boundary with the solid, conducting inner core will be neglected in this study, as it is thought the geodynamo operates chiefly outside of the tangent cylinder (an imaginary surface aligned with the rotation axis and circumscribing the inner core). The molten iron which makes up the outer core has a kinematic viscosity which is probably not dissimilar from that of water [11], and therefore may be taken as inviscid over the large lengthscales considered. The force balance is instead thought to be dominated by the effect of the rapid background rotation of the Earth at an angular velocity  $\Omega$  of approximately  $2\pi$  radians per day. It is well known that rapidly-rotating fluids have a tendency to evolve in a manner which is effectively two-dimensional, being independent of distance along the rotation axis [12,13], and therefore simplified models which presuppose this disposition are often employed in their study.

Motion in the outer core is thought to be stirred by vigorous convection, with thermally or compositionally buoyant material pushing radially outwards from the hot inner core. The convection is strongly-forced, meaning the distribution of density anomaly within the core is likely to be chaotic and span a vast range of scales. This raises questions for both the geodynamo as a whole, and the westward drift; how does the organised dipolar field structure emerge from this stochastic forcing, and how can it also produce the systematic drift observed at large scales?

At present, there exists two main schools of thought on the answer to this final question. Arguably the most popular model, due to Pais & Jault [14], invokes a large-scale eccentric gyre – or westward-directed jet – which advects the mean magnetic field. An alternative hypothesis [15–18], rests upon certain magnetohydrodynamic modes with an invariably westward phase velocity. Without remark upon the merits of either of the above models, a third possibility is here

53 put forward, underpinned by the hydrodynamic Rossby waves produced when a rapidly-rotating  
 54 fluid is forced to deviate from two-dimensionality by the presence of the container walls (in this  
 55 case, the core-mantle boundary). We introduce the quasi-geostrophic theory of these waves in §2,  
 56 deriving their governing equation for a general container geometry, and dispersive properties in a  
 57 canonical example. The waves are linked to westward drift in §3, supported by a simplistic initial  
 58 value problem. A similar problem is approached in §4, only in a spherical geometry much more  
 59 reminiscent of the Earth. The discussion of §5 appraises the value of Rossby waves as a possible  
 60 source of the observed westward drift.

## 61 2. Theory of Quasi-Geostrophic Rossby Waves

62 Consider the Earth's outer core to be an inviscid, incompressible fluid in a state of rapid bulk  
 63 rotation at an angular velocity  $\boldsymbol{\Omega} = \Omega \mathbf{e}_z$ , where  $\mathbf{e}_z$  is the unit vector in the axial direction of either  
 64 a Cartesian  $(x, y, z)$  or cylindrical polar  $(s, \phi, z)$  co-ordinate system. In either case, a subscript  
 65  $\perp$  denotes the component of a vector perpendicular to  $\mathbf{e}_z$ . In a reference frame rotating at  $\boldsymbol{\Omega}$ ,  
 66 the Eulerian fluid velocity is  $\mathbf{u}(\mathbf{x}, t)$ . The core-mantle boundary is represented by symmetric,  
 67 impermeable surfaces at  $z = \pm h(\mathbf{x}_\perp)$ ; for a spherical geometry of unit radius, one would have  
 68  $h = \sqrt{1 - s^2}$ .

### 69 (a) Kinematics and the QG approximation

70 In a bid to simplify the analysis, the so-called *quasi-geostrophic approximation* [19–21] is made. This  
 71 is in deference to the fact that the rapid background rotation forces the fluid to seek steady states  
 72 which are independent of the axial co-ordinate  $z$  (geostrophic). The presence of the boundaries at  
 73  $\pm h$  introduces small departures from geostrophy which cause these states to evolve on a timescale  
 74 much longer than the rotation period; such motions might be called quasi-geostrophic, though  
 75 the definition of the phrase is somewhat imprecise. Here, the term quasi-geostrophic (QG) is  
 76 used in a strict sense: as a label for the assumption that the velocity components perpendicular  
 77 to the rotation axis ( $\mathbf{u}_\perp$ ) are independent of the axial co-ordinate, an approach which has seen  
 78 much success in modelling of outer core convection [22–24]. This is despite the fact that the  
 79 assumption is only strictly valid when the boundary slope is small, a condition clearly violated in  
 80 the equatorial regions of the Earth's spherical core [21,25]. Moreover, the approximation remains  
 81 reasonable even in the presence of a background magnetic field [26].

82 The velocity field  $\mathbf{u}$  in this formulation is subject to three kinematic conditions:

- 83 (i) Incompressibility,  $\nabla \cdot \mathbf{u} = 0$ ;
- 84 (ii) Non-penetration at the upper and lower boundaries,  $(\nabla h \mp \mathbf{e}_z) \cdot \mathbf{u}|_{\pm h} = 0$ ;
- 85 (iii) The QG approximation,  $\mathbf{u}_\perp = \mathbf{u}_\perp(\mathbf{x}_\perp, t)$ .

86 It can be shown that a representation of the form

$$87 \quad \mathbf{u} = \nabla \chi \times \nabla \left( \frac{z}{h} \right) \quad (2.1)$$

88 fulfils these requirements, with the streamfunction  $\chi(\mathbf{x}_\perp, t)$  neatly encapsulating the evolution of  
 89 the vector field  $\mathbf{u}(\mathbf{x}, t)$  through a scalar function of just two spatial co-ordinates. Note that this  
 90 form is a generalisation of that introduced by Schaeffer and Cardin [20], which itself improves  
 91 upon the classical perturbation expansion approach (as discussed in [23]). Restricting solutions  
 92 to the form (2.1) offers a drastic simplification of the analysis, whilst providing a useful tool with  
 93 which to probe the physics of axially-elongated structures in the core of the Earth.

### 94 (b) Dynamics and governing equation

95 A governing equation for the streamfunction  $\chi$  in this QG approach is now derived. In a reference  
 96 frame rotating at the bulk angular velocity  $\boldsymbol{\Omega}$ , conservation of momentum for an inviscid,

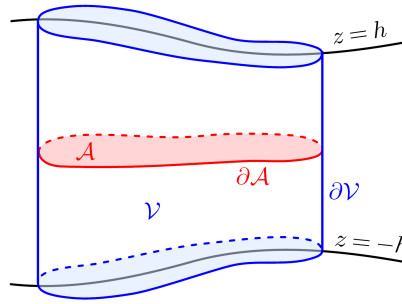


**Figure 1.** Schematic of the control volume considered when deriving the governing equation for a QG flow.

97 incompressible fluid may be written

$$98 \quad \frac{\partial \mathbf{u}}{\partial t} + \mathbf{u} \cdot \nabla \mathbf{u} + 2\boldsymbol{\Omega} \times \mathbf{u} = -\nabla \Pi \quad (2.2)$$

99 for some modified pressure  $\Pi$ . In the limit of small Rossby number ( $\mathcal{U} \ll \Omega \mathcal{L}$  for some  
100 characteristic velocity  $\mathcal{U}$  and lengthscale  $\mathcal{L}$ ), the second term (advection) may be neglected in  
101 comparison to the third (Coriolis). The curl of (2.2) then yields the equation

$$102 \quad \frac{\partial \boldsymbol{\omega}}{\partial t} = 2\boldsymbol{\Omega} \cdot \nabla \mathbf{u} \quad (2.3)$$

103 for the evolution of the vorticity  $\boldsymbol{\omega} = \nabla \times \mathbf{u}$ . Evidently, steady solutions must be independent of  
104 distance along the rotation axis (i.e. geostrophic) — this is the Taylor-Proudman theorem [12,13].  
105 However, in order to satisfy non-penetration at  $z = \pm h$ , QG solutions must possess a weak  $z$ -  
106 dependence, and therefore can exhibit unsteadiness. To derive an equation for the evolution of  
107 a QG flow, one could simply substitute the representation (2.1) into the axial component of the  
108 vorticity equation (2.3), a procedure commonly employed in the literature (e.g. [21,22]). However,  
109 as pointed out in Labbé *et al.* [27], a more efficacious approach is to instead project the momentum  
110 equation (2.2) onto flows of the QG form (2.1), thereby obtaining a reduced model which better  
111 approximates the dynamics. This has been verified analytically in a full sphere by Maffei *et al.* [25],  
112 who found remarkably good agreement with the fully three-dimensional solutions of Zhang *et al.* [28].  
113

114 We therefore proceed by following the derivation of Labbé *et al.* [27], generalising their  
115 results in a sphere to a more arbitrary geometry. Consider a control volume  $\mathcal{V}$  of fluid of  
116 constant horizontal cross section  $\mathcal{A}$ , bounded at the top and bottom by the caps  $z = \pm h(\mathbf{x}_\perp)$ . The  
117 boundaries of  $\mathcal{V}$  and  $\mathcal{A}$  are denoted  $\partial\mathcal{V}$  and  $\partial\mathcal{A}$  respectively (figure 1). After excluding advection,  
118 the momentum equation (2.2) is projected onto a QG trial function  $\mathbf{u}' = \nabla\chi' \times \nabla\left(\frac{z}{h}\right)$ , which by  
119 construction satisfies  $\chi'|_{\partial\mathcal{A}} = 0$ , then integrated over  $\mathcal{V}$ :

$$120 \quad \iiint_{\mathcal{V}} \mathbf{u}' \cdot \dot{\mathbf{u}} \, dV + 2\Omega \iiint_{\mathcal{V}} \mathbf{u}' \cdot (\mathbf{e}_z \times \mathbf{u}) \, dV = - \iiint_{\mathcal{V}} \mathbf{u}' \cdot \nabla \Pi \, dV, \quad (2.4)$$

121 with a dot over a quantity denoting a time derivative. Using the divergence theorem, the right  
122 hand side is equal to

$$123 \quad \iiint_{\mathcal{V}} \Pi \nabla \cdot \mathbf{u}' \, dV - \iint_{\partial\mathcal{V}} \Pi \mathbf{u}' \cdot d\mathbf{S} = 0 \quad (2.5)$$

124 since the choice of  $\chi'$  guarantees streamlines of  $\mathbf{u}'$  cannot pass through  $\partial\mathcal{V}$ . The contribution from  
125 the Coriolis term simplifies to

$$126 \quad 2\Omega \iiint_{\mathcal{V}} \mathbf{u}' \cdot (\mathbf{e}_z \times \mathbf{u}) \, dV = 2\Omega \iiint_{\mathcal{V}} \left( \frac{\mathbf{e}_z \times \nabla \chi'}{h^2} \right) \cdot \nabla \chi' \, dV. \quad (2.6)$$

The integration from  $z = -h$  to  $z = h$  can be completed, thereby projecting the equations onto the horizontal plane  $\mathcal{A}$ :

$$2\Omega \iiint_{\mathcal{V}} \mathbf{u}' \cdot (\mathbf{e}_z \times \mathbf{u}) \, dV = 4\Omega \iint_{\mathcal{A}} \left( \frac{\mathbf{e}_z \times \nabla \chi}{h} \right) \cdot \nabla \chi' \, dA \quad (2.7)$$

$$= 4\Omega \oint_{\partial \mathcal{A}} \chi' \left( \frac{\mathbf{e}_z \times \nabla \chi}{h} \right) \cdot \mathbf{n} \, ds - 4\Omega \iint_{\mathcal{A}} \chi' \nabla \cdot \left( \frac{\mathbf{e}_z \times \nabla \chi}{h} \right) \, dA \quad (2.8)$$

$$= 4\Omega \cdot \iint_{\mathcal{A}} \chi' (\nabla \frac{1}{h} \times \nabla \chi) \, dA. \quad (2.9)$$

This requires use of the two-dimensional version of the divergence theorem,

$$\iint_{\mathcal{A}} \nabla \cdot \mathbf{v} \, dA = \oint_{\partial \mathcal{A}} \mathbf{v} \cdot \mathbf{n} \, ds \quad (2.10)$$

(where  $\mathbf{n}$  is the in-plane unit outward normal to  $\partial \mathcal{A}$ ), then the fact that  $\chi'|_{\partial \mathcal{A}} = 0$ . A very similar procedure may be applied to the inertial term,

$$\iiint_{\mathcal{V}} \mathbf{u}' \cdot \dot{\mathbf{u}} \, dV = \iiint_{\mathcal{V}} \left( \frac{\nabla \dot{\chi}}{h^2} + z^2 \nabla \frac{1}{h} \times (\nabla \dot{\chi} \times \nabla \frac{1}{h}) \right) \cdot \nabla \chi' \, dV \quad (2.11)$$

$$= 2 \iint_{\mathcal{A}} \left( \frac{\nabla \dot{\chi}}{h} + \frac{h^3}{3} \nabla \frac{1}{h} \times (\nabla \dot{\chi} \times \nabla \frac{1}{h}) \right) \cdot \nabla \chi' \, dA \quad (2.12)$$

$$= -2 \iint_{\mathcal{A}} \chi' \nabla \cdot \left( \frac{\nabla \dot{\chi} + \frac{1}{3} \nabla h \times (\nabla \dot{\chi} \times \nabla h)}{h} \right) \, dA, \quad (2.13)$$

so equation (2.4) can be rewritten

$$\iint_{\mathcal{A}} \chi' \left[ \nabla \cdot \left( \frac{\nabla \dot{\chi} + \frac{1}{3} \nabla h \times (\nabla \dot{\chi} \times \nabla h)}{h} \right) + 2\Omega \cdot (\nabla \chi \times \nabla \frac{1}{h}) \right] \, dA = 0. \quad (2.14)$$

Since this must be satisfied for all possible choices of the trial function  $\chi'$ , the streamfunction  $\chi$  must obey the governing equation

$$\nabla \cdot \left( \frac{\nabla \dot{\chi} + \frac{1}{3} \nabla h \times (\nabla \dot{\chi} \times \nabla h)}{h} \right) + 2\Omega \cdot (\nabla \chi \times \nabla \frac{1}{h}) = 0. \quad (2.15)$$

Note that the second term inside the divergence is the sole difference between this equation and the axial vorticity formulation (i.e. plugging (2.1) into the  $z$ -component of (2.3)); for moderate values of  $\nabla h$ , however, this difference becomes significant.

### (c) QG Rossby waves

The governing equation (2.15) can support oscillatory solutions known as QG Rossby waves, in analogy to their atmospheric counterparts [15,29], discussed in detail by Vallis [30], for example. The theory of QG Rossby waves in the Earth's interior mirrors this classical analysis — to extract their archetypal form, select Cartesian co-ordinates  $(x, y, z)$  and a linear height profile  $h(y) = H + h'y$  for positive constants  $H$  and  $h'$ , the domain height and slope respectively. This aims to capture the slope of the core-mantle boundary at zero order, with the  $x$ -axis oriented east and the  $y$ -axis radially inwards. Furthermore, the slope is for the moment assumed small (in comparison to the aspect ratio of the QG structures), so (2.15) may be written in the linearised form

$$\frac{\partial}{\partial t} \nabla^2 \chi \approx \frac{2\Omega h'}{H} \frac{\partial \chi}{\partial x}. \quad (2.16)$$

Note that an equivalent equation could also stem from the axial vorticity formulation, or indeed a perturbation expansion approach [31]. Seek travelling wave solutions of the form  $\chi(x, y, t) \propto \exp\{i(\mathbf{k}_{\perp} \cdot \mathbf{x}_{\perp} - \varpi(\mathbf{k}_{\perp})t)\}$  with frequency  $\varpi$  and wavevector  $\mathbf{k}_{\perp} = [k_x, k_y, 0]^T =$

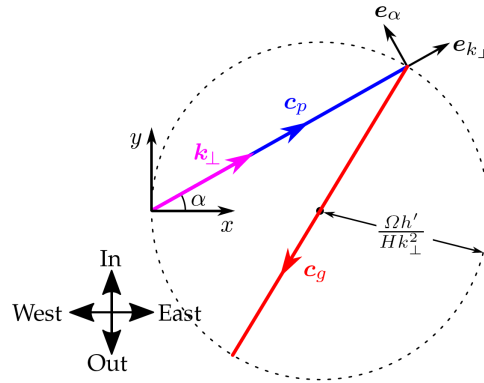


**Figure 2.** Velocity diagram for QG Rossby waves when  $h = H + h'y$  for small  $h'$ . Phase velocity  $c_p$  is related to group velocity  $c_g$  for a given choice of  $k_{\perp}$ . The rotation axis is out of the page, and the labelled directions orient the figure within the Earth's outer core.

150  $k_{\perp} [\cos \alpha, \sin \alpha, 0]^T$ , where  $\alpha$  is the angle between the wavevector and the  $x$ -axis and  $k_{\perp} = |k_{\perp}|$ .  
 151 This yields the dispersion relationship for QG Rossby waves,

$$152 \quad \varpi = \frac{2\Omega h'}{H k_{\perp}} \cos \alpha. \quad (2.17)$$

153 Writing  $e_{k_{\perp}}$  for the unit vector in the direction of  $k_{\perp}$  and  $e_{\alpha}$  for the unit vector in the direction  
 154 of increasing  $\alpha$  (figure 2), the phase velocity corresponding to (2.17) can be expressed as

$$155 \quad c_p = \frac{\varpi}{k_{\perp}} e_{k_{\perp}} = \frac{2\Omega h'}{H k_{\perp}^2} \cos \alpha e_{k_{\perp}}. \quad (2.18)$$

156 Note that the component of phase velocity in the  $x$ -direction is always positive, meaning wave  
 157 crests invariably progress eastwards. However, the same is not true for the wave energy, which  
 158 instead propagates at the group velocity, given by the gradient in  $k_{\perp}$ -space of the frequency,

$$159 \quad c_g = \frac{\partial \varpi}{\partial k_{\perp}} e_{k_{\perp}} + \frac{1}{k_{\perp}} \frac{\partial \varpi}{\partial \alpha} e_{\alpha} = -\frac{2\Omega h'}{H k_{\perp}^2} (\cos \alpha e_{k_{\perp}} + \sin \alpha e_{\alpha}). \quad (2.19)$$

160 The relationship between the phase and group velocities is best understood diagrammatically;  
 161 figure 2 is a velocity diagram relating the two, similar to the plots of Duba & McKenzie [32]. The  
 162 magnitude of  $c_g$  is independent of  $\alpha$ , so on the velocity diagram the vector  $c_g$  is the diameter of  
 163 a circle of radius  $\Omega h' / H k_{\perp}^2$ . Furthermore,  $(c_p + c_g) \cdot c_p = 0$ , so  $c_p$  is a chord of the same circle  
 164 terminating at the base of  $c_g$ . Since  $c_p$  is always in the positive  $x$  direction, the circle must lie to  
 165 the right of the origin as shown.

166 Using figure 2, it is possible to probe the effect of varying the wavevector orientation  $\alpha$  for a  
 167 given  $k_{\perp}$  (i.e. a specified horizontal length scale). Consider only positive frequencies ( $-\frac{\pi}{2} < \alpha \leq$   
 168  $\frac{\pi}{2}$ ), for which figure 2 makes sense. The phase velocity vector  $c_p$  is constrained to move along the  
 169 dashed circle, whereas the group velocity vector  $c_g$  starts where  $c_p$  finishes and is necessarily a  
 170 diameter of the same circle. Although the phase velocity always has a positive  $x$ -component, the  
 171 group velocity shows no such preference. In fact, the  $x$ -component of  $c_g$  is negative (westward)  
 172 for  $|\alpha| < \frac{\pi}{4}$  and positive (eastward) for  $|\alpha| > \frac{\pi}{4}$ . When  $\alpha = 0$ ,  $c_p$  and  $c_g$  are exactly opposite, so  
 173 an observer following a wave group moving westward would see wave crests heading in the  
 174 opposite direction at twice the speed of the group. When  $\alpha = \frac{\pi}{2}$  the group velocity remains finite  
 175 (and due east) despite the fact the waves have no phase velocity. Waves with  $\alpha = \frac{\pi}{4}$  propagate  
 176 directly outwards and waves with  $\alpha = -\frac{\pi}{4}$  inwards.

177 The dependence of wave velocity on  $k_{\perp}$  is comparatively trivial; waves with longer  
 178 wavelengths (smaller  $k_{\perp}$ ) travel faster. As  $|c_g| \sim k_{\perp}^{-2}$ , the waves are highly dispersive.

### 179 3. QG Rossby waves and the westward drift

180 A possible explanation for the westward drift of the Earth's magnetic field at the core-mantle  
 181 boundary based upon this classical theory of hydrodynamic QG Rossby waves is now offered.  
 182 Suppose, not unreasonably, that the fluid outer core is stirred by gravitating buoyant anomalies,  
 183 which constitute localised disturbances to the system in the form of convective upwellings or  
 184 plumes. Consider one such disturbance introduced at a location outside of the tangent cylinder  
 185 (i.e. not directly north or south of the solid inner core). The disturbance will in general be  
 186 three-dimensional, but the velocity field it instigates will rapidly become elongated along the  
 187 rotation axis through the action of inertial waves [33], and therefore quasi-geostrophic after a  
 188 short transient period. It is thus useful to consider a thought experiment posed as an initial value  
 189 problem in which a localised QG velocity field is specified as an initial condition, and the flow  
 190 allowed to evolve as an assemblage of QG Rossby waves, operating on a timescale much longer  
 191 than the rotation period.

192 A generic initial condition will excite a broad spectrum of waves – that is to say, many different  
 193 choices of wavevector  $\mathbf{k}_\perp$  – which will all spread from the source according to their individual  
 194 dispersive properties. A disturbance of characteristic size  $\ell$  will have a spectrum peaked  
 195 around a wavevector magnitude  $k_\perp$  of order  $\ell^{-1}$ , but will in general excite wavevectors of all  
 196 possible orientations  $\alpha$ . Therefore, consider the dependence of the group velocity on wavevector  
 197 orientation by referring back to figure 2. For wavevectors with  $\alpha \approx \pm \frac{\pi}{2}$ , corresponding to  
 198 structures elongated in the east-west direction, the group velocity is east; for wavevectors with  
 199  $\alpha \approx 0$ , i.e. structures elongated in the radial direction, the group velocity is west. QG Rossby waves  
 200 therefore disperse in a manner which segregates different spatial structures from an arbitrary  
 201 initial disturbance, with east-west extended features heading east and radially extended features  
 202 west.

203 However, it is unreasonable to assume the excitation of these waves in the core of the  
 204 Earth is arbitrary. For motions continually stirred by vigorous convection, one might expect the  
 205 proliferation of sinuous radial plumes, emanating from the inner core and being much longer  
 206 than they are wide. Such structures commonly arise in numerical and experimental studies of  
 207 core dynamics (e.g. [34,35]). Due to the constraint imposed by the rapid background rotation,  
 208 such plumes would also be elongated in the axial direction, forming a series of radial sheets  
 209 which are likely to be well-represented by the QG approximation [36]. In the context of our  
 210 thought experiment, a radial sheet (extended in the  $y$ -direction) will possess much more energy  
 211 in wavevectors pointing east-west ( $\alpha \approx 0$ ) than radially ( $\alpha \approx \pm \frac{\pi}{2}$ ). When the solution to such an  
 212 initial value problem is evolved, the abundance of wavevectors with  $\alpha \approx 0$  will dominate the  
 213 picture. Since the group velocity for these solutions is in the negative  $x$  direction, a radially-  
 214 extended disturbance will preferentially transmit energy to the west, making this class of QG  
 215 Rossby waves an intriguing candidate for the mechanism underlying westward drift.

#### 216 (a) Demonstration through a model problem

217 To support the arguments made so far, consider a simplistic model problem which demonstrates  
 218 the ability of QG Rossby waves to segregate different spatial structures. The canonical equation  
 219 (2.16) is solved in a domain which is infinite in  $x$  and  $y$ , starting from some initial condition  
 220  $\chi(\mathbf{x}_\perp, t=0) = \chi_{\text{init}}(\mathbf{x}_\perp)$ , by taking a two-dimensional spatial Fourier transform. Emphasis is  
 221 placed upon the significance of the choice of initial condition, which is constrained to be of the  
 222 form

$$223 \chi_{\text{init}} = \exp \left\{ -\frac{1}{2} \left( \frac{x^2}{\ell_x^2} + \frac{y^2}{\ell_y^2} \right) \right\}. \quad (3.1)$$

Since contours of  $\chi$  are equivalent to streamlines in the equatorial plane, this corresponds to a  
 columnar vortex of extent  $\ell_x$  in the  $x$ -direction and  $\ell_y$  in the  $y$ -direction. Using  $\sqrt{\ell_x \ell_y}$  as the  
 unit of length, the solution to the initial value problem may be written as the two-dimensional

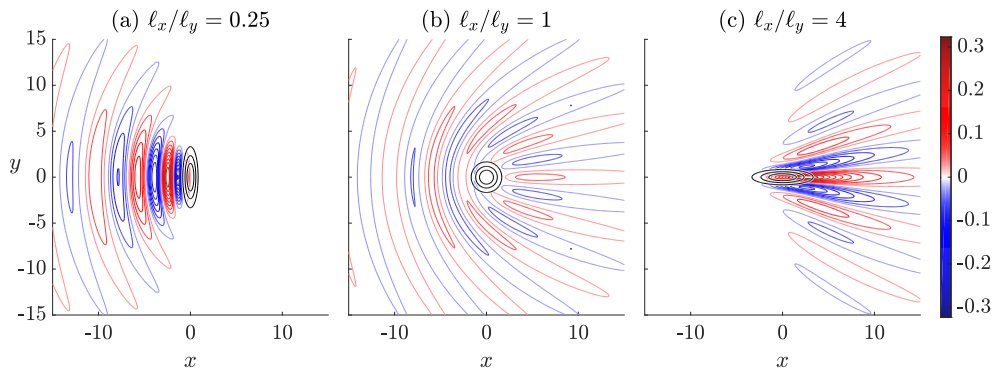


**Figure 3.** Solutions to the canonical QG Rossby wave equation (2.16) for a simple initial value problem starting from (3.1). The height of the container is  $h = H + h'y$ . Contours of streamfunction  $\chi$  are plotted at  $\frac{2\Omega h't}{H} = 15$  for three different choices of aspect ratio, and black contours are at quartiles of the initial condition. Lengths are in units of  $\sqrt{\ell_x \ell_y}$ .

dispersion integral

$$\chi(\mathbf{x}_\perp, t) = \frac{2}{\pi} \int_0^{\pi/2} \int_0^\infty k_\perp \exp \left\{ -\frac{1}{2} k_\perp^2 \left( \ell_x^2 \cos^2 \alpha + \ell_y^2 \sin^2 \alpha \right) \right\} \times \cos \left( \left[ k_\perp x - \frac{2\Omega h't}{H k_\perp} \right] \cos \alpha \right) \cos(k_\perp y \sin \alpha) dk_\perp d\alpha, \quad (3.2)$$

224 wherein  $k_\perp$  and  $\alpha$  have the same interpretations as in the dispersion relation (2.17). This  
 225 expression is evaluated numerically for three different choices of the initial condition's aspect  
 226 ratio  $\ell_x/\ell_y$  (figure 3). The central pane shows the case of an axisymmetric initial condition, which  
 227 excites waves of all orientations  $\alpha$  equally and therefore shows no preferential direction for energy  
 228 transport, although the partition of different spatial structures is visible. The left pane shows the  
 229 case of a radially-extended initial condition, four times longer in the direction of the slope than it  
 230 is wide; the bias towards westward-propagating waves is self-evident. For completeness, the right  
 231 pane features an initial condition which is elongated in the east-west direction, which exhibits a  
 232 strong preference for eastward propagation. It is worth remarking that the aspect ratio need not  
 233 be extreme for this effect to be apparent; it is very clear-cut here even for a moderate value of 4:1.

#### 234 4. A model problem: westward-propagating waves in a sphere

235 It has been established so far that, in the case of a gentle slope, the linearised equation (2.16)  
 236 supports wave motions which partition different spatial structures — crucially, with flows  
 237 elongated in the direction of the slope going west. However, it is not obvious that the same will  
 238 necessarily hold true for a more complicated geometry with an appreciable slope, such as that  
 239 presented by the core-mantle boundary. Therefore, consider an initial value problem similar to  
 240 that of the previous section, but in an enclosed spherical geometry reminiscent of the Earth's core.  
 241 A full sphere – deficient of the solid inner core – is used in order to simplify the analysis. First,  
 242 mode shapes and frequencies are derived in this geometry, following Maffei *et al.* [25], before the  
 243 calculated modes are used to solve an illustrative initial value problem.

244 Despite the spherical geometry, cylindrical polar coordinates  $(s, \phi, z)$  – with  $s$  being the radial  
 245 location,  $\phi$  the azimuthal angle, and  $z$  the distance along the rotation axis – are adopted in order

246 to usefully apply the QG approximation. Taking lengths in units of outer core radii, the governing  
 247 equation is then (2.15) with the axisymmetric height profile  $h(s) = \sqrt{1 - s^2}$ :

$$248 \left[ \frac{\partial}{\partial s} \left( \frac{s}{h} \frac{\partial}{\partial s} \right) + \frac{1}{hs} \left( 1 + \frac{s^2}{3h^2} \right) \frac{\partial^2}{\partial \phi^2} \right] \frac{\partial \chi}{\partial t} - \frac{2\Omega s}{h^3} \frac{\partial \chi}{\partial \phi} = 0. \quad (4.1)$$

249 First, note that any solution satisfying  $\frac{\partial \chi}{\partial t} = \frac{\partial \chi}{\partial \phi} = 0$  will be a particular integral of this equation.  
 250 This corresponds to the steady, strictly geostrophic motion of coaxial cylinders ( $\mathbf{u} = u_\phi(s)\mathbf{e}_\phi$ );  
 251 hence, the axisymmetric component of any initial condition will not evolve, and one need only  
 252 solve (4.1) for the non-axisymmetric portion of the flow. This can be done by seeking normal mode  
 253 solutions of the form

$$254 \chi(s, \phi, t) = \mathbb{R} \{ \bar{\chi}(s) \exp(i[m\phi - \varpi t]) \} \quad (4.2)$$

255 for some azimuthal wavenumber  $m$  and modal frequency  $\varpi$ , with  $\mathbb{R}\{\cdot\}$  denoting the real part of  
 256 a quantity. This turns (4.1) into an ordinary differential equation for the radial mode shape,

$$257 \frac{d}{ds} \left( \frac{s}{h} \frac{d\bar{\chi}}{ds} \right) + \left[ \frac{2\Omega ms}{\varpi h^3} - \frac{m^2}{hs} \left( 1 + \frac{s^2}{3h^2} \right) \right] \bar{\chi} = 0, \quad (4.3)$$

258 which must be solved subject to boundary conditions at the origin ( $s=0$ ) and the equatorial  
 259 boundary ( $s=1$ ). Regularity at the origin requires  $\bar{\chi} \sim s^m$  as  $s \rightarrow 0$ , whereas non-penetration at  
 260 the outer boundary requires

$$261 u_s|_{s=1} = \lim_{s \rightarrow 1} \left( \frac{1}{hs} \frac{\partial \chi}{\partial \phi} \right) = 0. \quad (4.4)$$

262 Since  $\chi$  is a streamfunction, its constant value at the outer boundary can be chosen, so is set at zero;  
 263 more specifically, we must have  $\bar{\chi}(s \rightarrow 1) \sim h^3$  in order for  $u_s = \frac{1}{hs} \frac{\partial \chi}{\partial \phi}$  to be zero and  $u_\phi = -\frac{1}{h} \frac{\partial \phi}{\partial s}$   
 264 to be finite at the outer boundary. The solution to the eigenvalue problem posed by (4.3) and these  
 265 boundary conditions is given in Maffei *et al.* [25]; the mode shapes are of the form

$$266 \bar{\chi}_n^m(s) = s^m h^3 P_{n-1}^{(3/2, m)}(2s^2 - 1) \quad (4.5)$$

267 and the corresponding frequencies are

$$268 \varpi_n^m = \frac{m}{n(2n + 2m + 1) + m/2 + m^2/6}. \quad (4.6)$$

269 Here,  $n \geq 1$  is the radial mode number, equal to the number of turning points of  $\bar{\chi}_n^m$  within the  
 270 domain. The mode shapes are expressed in terms of Jacobi polynomials  $P_V^{(\alpha, \beta)}(x)$  [37]. Note that,  
 271 for all  $m \geq 1$ , the frequency  $\varpi_n^m$  is positive, meaning all modes revolve in a prograde (eastward)  
 272 sense; this is analogous to the observation that the phase velocity in the Cartesian problem (2.18)  
 273 is always in the positive  $x$ -direction. Just as in that problem, this does not preclude the possibility  
 274 that the energy from a localised disturbance can nevertheless propagate west, as demonstrated  
 275 below.

276 The general solution to (4.1) (setting aside the axisymmetric particular integral for a moment)  
 277 can be written as an infinite sum of the above modes,

$$278 \chi(s, \phi, t) = \mathbb{R} \left\{ \sum_{m=1}^{\infty} \sum_{n=1}^{\infty} C_n^m \bar{\chi}_n^m(s) e^{i(m\phi - \varpi_n^m t)} \right\} \quad (4.7)$$

279 for some complex coefficients  $C_n^m$  to be determined by the initial condition  $\chi_{\text{init}}(s, \phi)$ . In fact, it  
 280 can be seen from the self-adjoint equation (4.3) that the radial mode shapes (4.5) are orthogonal

281 with respect to the function  $s/h^3$ , i.e.

$$282 \int_0^1 \frac{s}{h^3} \bar{\chi}_n^m(s) \bar{\chi}_{n'}^m(s) ds = 0 \quad \text{for } n \neq n', \quad (4.8)$$

283 which enables the derivation of an expression for each modal coefficient as an integral over the  
284 equatorial plane,

$$285 C_n^m = \frac{\int_0^1 \frac{s}{h^3} \bar{\chi}_n^m(s) \oint \chi_{\text{init}}(s, \phi) e^{-im\phi} d\phi ds}{\pi \int_0^1 \frac{s}{h^3} [\bar{\chi}_n^m(s)]^2 ds}. \quad (4.9)$$

286 All that remains is the axisymmetric portion of the flow, given simply by

$$287 \chi_{\text{ax}}(s) = \frac{1}{2\pi} \oint \chi_{\text{init}}(s, \phi) d\phi. \quad (4.10)$$

288 This analysis allows the solution of an illustrative initial value problem, similar to that of section  
289 3, by using (4.9) to express the initial condition as a linear sum of modes and solving for the  
290 streamfunction at a later time by evaluating the sums in (4.7) truncated at finite  $m$  and  $n$ .

### 291 (a) Choice of initial condition

292 If the simple Cartesian cartoon discussed in section 3 is to be believed, the choice of initial  
293 condition, and therefore distribution of energy in  $k_{\perp}$ -space (or equivalently, between modes),  
294 will have a profound effect on the direction of net energy propagation. In fact, those modes for  
295 which the frequency  $\varpi_n^m$  in (4.6) is a decreasing function of  $m$  will be associated with westward  
296 propagation of energy; in the Cartesian case,  $c_{g,x}$  is negative for  $\partial\varpi/\partial k_x < 0$ , and analogously  
297 retrograde group velocity is seen in the sphere for  $\partial\varpi_n^m/\partial m < 0$ , i.e.

$$298 m > \sqrt{6n(1+2n)}. \quad (4.11)$$

299 For a westward drift to be observed in this model problem, the harmonic content of the  
300 initial condition must be biased towards modes which satisfy this inequality. For definiteness,  
301 discussion is restricted to the form of initial condition

$$302 \chi_{\text{init}}(s, \phi) = h^3 s \exp \left\{ -\frac{1}{2} \left( \frac{(s-s_0)^2}{\ell_s^2} + \frac{s_0^2 \phi^2}{\ell_\phi^2} \right) \right\}. \quad (4.12)$$

303 This is essentially a columnar Gaussian vortex, as for the model problem of section 3, with the  
304 pre-multiplying factor  $h^3 s$  ensuring the boundary conditions are satisfied at from the outset. It is  
305 broadly unimportant exactly what form the initial condition takes, however — it is the general  
306 distribution of energy between modes which will dictate the solution's character.

307 There are three controlling lengths in the initial condition (4.12); the radial and azimuthal  
308 extents of the vortex  $\ell_s$  and  $\ell_\phi$ , and the radial location of the vortex centre  $s_0$ . In search of a  
309 westward bias to energy propagation, the parameters  $\ell_s = 0.1$ ,  $\ell_\phi = 0.01$  and  $s_0 = 0.7$  are selected,  
310 giving a slender radially-extended structure near the middle of the outer core region  $0.35 < s < 1$   
311 (though there is no inner core boundary in this calculation). The solution is expressed as a finite  
312 sum of modes (i.e. a truncated version of (4.7)) by evaluating the integrals (4.9) for the coefficients  
313  $C_n^m$  numerically. Due to the narrowness of the initial condition, more modes of high azimuthal  
314 wavenumber are required; the ranges  $m \leq 200$  and  $n \leq 50$  are used.

### 315 (b) Westward bias to energy propagation in a sphere

316 Figure 4 shows the solution to the initial value problem evaluated at  $\Omega t = 2 \times 10^4$  ( $t = 8.7\text{yr}$ ).  
317 Streamlines in the equatorial plane are produced by plotting contours of  $\chi$ , with the black  
318 contours corresponding to the initial value (4.12). Although this solution is many times more  
319 complicated than the Cartesian problem of figure 3, there remains a striking preference for wave  
320 propagation to the west of the initial disturbance. This is despite the fact that each individual  
321 eigenmode has an eastward phase velocity; it is the superposition of modes which creates the

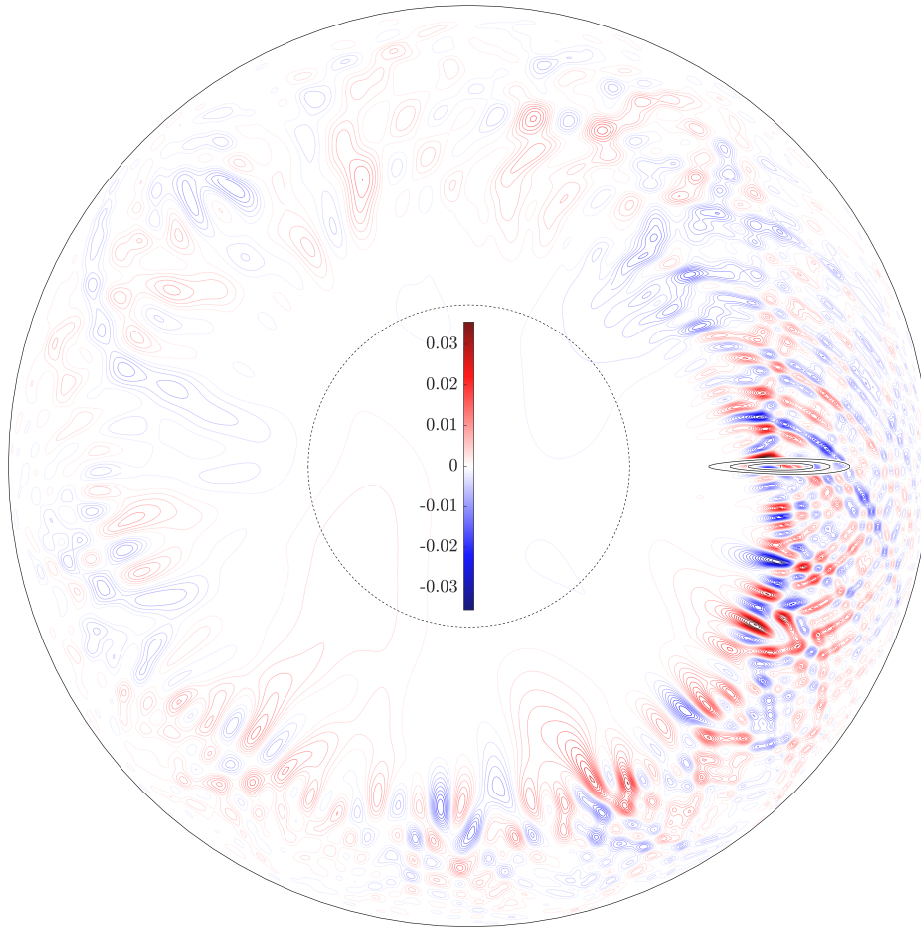


**Figure 4.** Contours of  $\chi$  (i.e. streamlines in the equatorial plane, viewed from the north) at  $\Omega t = 2 \times 10^4$  for an initial value problem starting from a radially extended vortex (4.12) with  $\ell_s = 0.1$ ,  $\ell_\phi = 0.01$ , and  $s_0 = 0.7$ . Solid black contours are at quartiles of the initial condition, and the dashed black line shows the would-be location of the solid inner core.

322 visible westward bias. Wave motion appears to be confined to a circular band near the initial  
 323 radial location  $s_0$ , with little activity very close to the outer boundary or near the rotation axis.  
 324 The dashed line is at  $s = 0.35$ , where the inner core would be if it were included in the model;  
 325 thankfully, the vast majority of activity occurs outside of this region.

326 The preference for westward propagation may be understood in exactly the same way as the  
 327 Cartesian problem of section 3, but with the small slope assumption now relaxed. The majority of  
 328 the energy from the radially-extended initial condition is contained in modes with large azimuthal  
 329 wavenumbers, which conspire to produce a westward group velocity despite individually having  
 330 eastward phase velocities. To demonstrate that the former prevails, consider the distribution of  
 331 energy in the sphere as a function of longitude and time. Namely, the meridionally-averaged  
 332 specific kinetic energy,

$$333 \quad \left\langle \frac{1}{2} \mathbf{u}^2 \right\rangle (\phi, t) = \int_0^1 \left( \int_{-h}^h \frac{1}{2} \mathbf{u}^2 dz \right) s ds = \int_0^1 \frac{s}{h} \left[ (\nabla \chi)^2 + \frac{1}{3} (\nabla \chi \times \nabla h)^2 \right] ds, \quad (4.13)$$

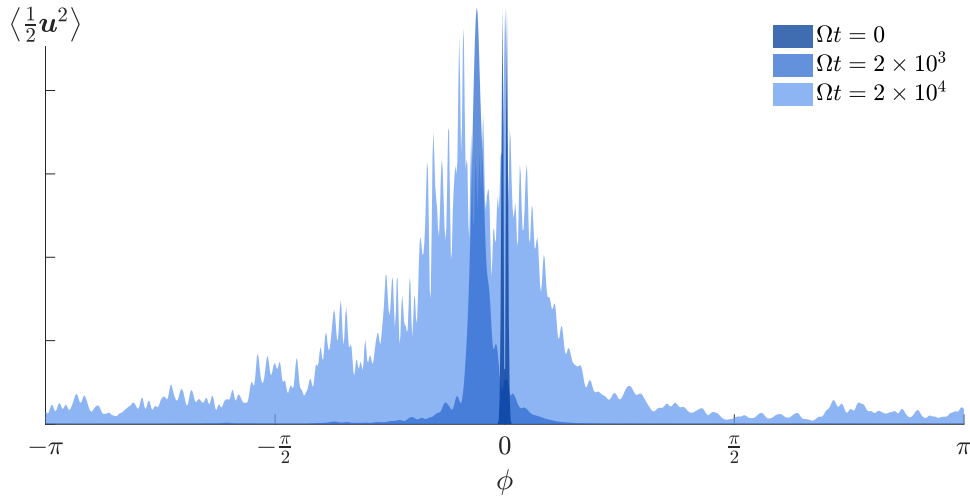


**Figure 5.** Specific kinetic energy, averaged over meridional slices, as a function of longitude  $\phi$  for the initial condition and two later times  $\Omega t = 2 \times 10^3$  and  $\Omega t = 2 \times 10^4$ . Plots are normalised to have the same maxima, though in actuality contain equal areas.

334 is evaluated as a function of  $\phi$  at a few choice times (figure 5). The energy, initially localised around  
 335  $\phi = 0$ , is almost all at negative  $\phi$  when  $\Omega t = 2 \times 10^3$ , and is still sharply peaked as the waves have  
 336 had little time to disperse. Come  $\Omega t = 2 \times 10^4$ , which corresponds to figure 4, the energy is much  
 337 more dispersed but retains its westward bias; of course, reflections and circumnavigations mean  
 338 a little energy does end up to the east of the initial disturbance.

## 339 5. Discussion

340 The model problems above successfully demonstrate the possibility for westward transport of  
 341 energy by hydrodynamic QG Rossby waves, but are intended as a proof-of-concept rather than  
 342 an accurate representation of core dynamics. Clearly, the flow in the Earth's outer core isn't  
 343 the solution to an initial value problem, but rather the result of continual convective stirring;  
 344 the interplay between buoyancy and velocity fields will introduce complexity beyond the scope  
 345 of this study (see [24]). However, the present theory demonstrates that westward propagation  
 346 requires only the prevalence of radial plumes, which are likely to be robustly generated by the  
 347 buoyant upwellings associated with strongly forced convection.

348 Indeed, discussions of vigorously forced convection are intrinsically linked to the relevant  
 349 smallest lengthscale in the core of the Earth, which is itself pertinent to dynamo action [38].  
 350 The thickness of the radial plumes will have a strong bearing on the propagation speed of their  
 351 associated wave packets, since the magnitude of the group velocity (2.19) is proportional to  
 352 the square of the wavelength, meaning narrower structures propagate much slower. The most  
 353 strongly-forced simulations to date (e.g. [34]) show structures more slender than those considered  
 354 in the model problem of figure 4, and it is not unreasonable to suspect that the true lengthscale is  
 355 even smaller. In fact, it is possible to infer this lengthscale under the assumption that QG Rossby  
 356 waves are responsible for the westward drift. From the expression for group velocity (2.19), the  
 357 speed of a wavepacket at a certain cylindrical radius  $s$  is given by

$$358 \quad |c_g| \approx \frac{2\Omega}{hk_{\perp}^2} \left| \frac{dh}{ds} \right| = \frac{2\Omega s}{(hk_{\perp})^2}. \quad (5.1)$$

359 For an azimuthally-propagating wavepacket, the angular velocity about the rotation axis is  
 360  $|c_g|/s$ ; equating this to the observed drift rate of the magnetic field  $D$  gives an expression for  
 361 the dominant wavelength of the packet,

$$362 \quad \lambda \approx 2\pi h \sqrt{\frac{D}{2\Omega}}. \quad (5.2)$$

363 Using a drift rate of  $0.27^\circ$  per year [5] and a radial location of the wavepacket  $s \sim 2000\text{km}$  gives  
 364 the estimate  $\lambda \sim 18\text{km}$ , a conceivable value for the prevalent scales in the Earth's core, but one  
 365 which should be treated with caution. Firstly, it is within touching distance of the Rhines length  
 366  $\sqrt{Uh/\Omega}$  ( $\sim 6\text{km}$  for  $U \sim 1\text{mm/s}$ ), at which the advection term in (2.2) becomes significant and  
 367 mean flows may arise. Secondly, the aspect ratios of such structures would be improbably large  
 368 for their coherence to be maintained over secular timescales. It seems more reasonable that in  
 369 truth  $\lambda$  is greater, with additional factors – interactions with the buoyancy and magnetic fields,  
 370 large values of boundary slope, or departures from quasi-geostrophy – acting to slow the wave  
 371 groups down. Unfortunately, the machinery required to investigate these non-linear phenomena  
 372 lies beyond our present scope.

373 Nevertheless, it seems remiss that so far no consideration has been given to the magnetic field,  
 374 despite the fact that the observed westward drift of its large scale features is the motivation for  
 375 this study. It is therefore necessary to ask what could link hydrodynamic QG Rossby waves  
 376 to the apparent motion of the spherical radial magnetic field  $B_r$  at the core-mantle boundary.  
 377 Since the drift is observed to be mainly in the equatorial regions [8], motion of the *cylindrical*  
 378 radial field  $B_s$ , which will be approximately equal to  $B_r$  at low latitudes, is discussed instead.  
 379 To a first approximation, magnetic field lines may be thought of as material curves, pinned  
 380 into the fluid at all points [29,39], so there are essentially two ways of modifying the radial  
 381 magnetic field: advection and stretching of an existing  $B_s$  by a mean flow, or rotation of the  
 382 other components ( $B_\phi, B_z$ ) by transverse gradients in radial velocity ( $\partial_\phi u_s, \partial_z u_s$  respectively);  
 383 both mechanisms are discussed in the context of westward drift by Finlay [40] and Aubert *et*  
 384 *al.* [41]. Westward-propagating QG Rossby waves, which necessarily consist of radially-extended  
 385 sheet-like structures, have small azimuthal velocities so are unlikely to advect  $B_s$  strongly enough  
 386 to account for the westward drift. The radial velocity is much greater, but has small derivatives  
 387 in  $s$  and  $z$  so stretching of an existing  $B_s$  or shearing of  $B_z$  are both unlikely mechanisms. The  
 388 best candidate for generation of  $B_s$  is therefore shearing of  $B_\phi$  by azimuthal gradients in  $u_s$ ,  
 389 which are large for the slender radial jets. Furthermore, the azimuthal magnetic field is likely to  
 390 be relatively strong within the core [42], and largest at mid- to low-latitudes – which could explain  
 391 the equatorial bias to the observed drift, since a low-latitude  $B_\phi$  swept out by a QG radial jet  
 392 would produce a radial field anomaly at the core-mantle boundary in the vicinity of the equator.

393 At first glance, this argument appears to suffer from the deficiency that the manipulation of  
 394  $B_s$  occurs on the small scale of the wavelength  $\lambda$ , whereas the observed drift occurs in magnetic  
 395 field features hundreds of kilometres across. However, the observations themselves are hampered  
 396 by a lack of spatial resolution, so small-scale features simply aren't visible, even though they  
 397 may in fact contain a significant portion of the energy [4]. The observations instead feature large,  
 398 westward-moving patches [8] which one might compare to wave groups, with the small-scale  
 399 details (wave crests and troughs) within each patch unavailable. It is therefore to be expected  
 400 that, if the present theory were to explain the observations, large magnetic field features would  
 401 appear to be advected at the group (rather than phase) velocity of QG Rossby wave packets.

402 The feedback of the magnetic field on the dynamics through the action of the Lorentz force  
 403 has been ignored in this study. Indeed, for highly simplified field configurations it has been  
 404 shown that its inclusion introduces additional oscillations known as *slow magnetic Rossby waves*  
 405 which themselves have been suggested as a possible source of magnetic field drift since their  
 406 phase velocity is always westward [15–18]. However, these slow solutions coexist with others  
 407 known as *fast magnetic Rossby waves*, which are little more than a weakly-modified version of the  
 408 hydrodynamic solutions discussed at length above. The perturbation to the magnetic field does

not strongly influence the dynamics of these waves, and so they remain an equally viable source of westward drift, with the magnetic field approximating a passive tracer at leading order.

Moreover, the fact that the dynamics of QG Rossby waves are independent of the magnetic field configuration and magnitude is a strength of the present theory. Slow magnetic Rossby modes have to date only been demonstrated for simple choices of background field [21,27], and it is therefore unclear whether such solutions are meaningful in a geophysical context. Conversely, the fast (i.e. hydrodynamic) solutions are likely to persist regardless of the magnetic field structure, meaning they are an almost unavoidable feature of QG flows in the Earth's outer core. This robustness tallies with the observation of westward drift as a systematic component of the geomagnetic secular variation, and the fact that the waves operate on a scale much smaller than the observed field features may explain the broad scale-independence of the observed drift rate. These advantages, along with those discussed above, lend credibility to the theory presented here – that hydrodynamic QG Rossby waves with radially-extended structures may underpin the westward drift present in geomagnetic secular variation records.

**Data Accessibility.** This article has no additional data.

**Competing Interests.** The author has no competing interests.

**Ethics.** This study raised no ethical issues.

**Funding.** The author is funded by an EPSRC Doctoral Training Award. The majority of this work was completed during an academic visit to ETH Zürich, funded by a David Crighton fellowship from the Department of Applied Mathematics and Theoretical Physics, University of Cambridge.

**Acknowledgements.** I am grateful to Andrew Jackson and the EPM group at ETH Zürich for hosting me for a two-month academic visit in autumn 2017. Helpful suggestion for improvements to this manuscript were provided by Jack Atkinson, Peter Davidson, Andrew Jackson, Ben McDermott and two anonymous reviewers.

## References

- Halley E. 1692 An account of the cause of the change of the variation of the magnetical needle. with an hypothesis of the structure of the internal parts of the earth: as it was proposed to the Royal Society in one of their late meetings. *Philosophical Transactions* **17**, 563–578. (doi:10.1098/rstl.1686.0107).
- Bullard EC, Freeman C, Gellman H, Nixon J. 1950 The westward drift of the Earth's magnetic field. *Phil. Trans. R. Soc. Lond. A* **243**, 67–92. (doi:10.1098/rsta.1950.0014).
- Jackson A, Finlay C. 2015 Geomagnetic Secular Variation and Its Applications to the Core. In Schubert G, editor, *Treatise on Geophysics (Second Edition)* pp. 137–184. Oxford: Elsevier. (doi:10.1016/B978-0-444-53802-4.00099-3).
- Holme R, Olsen N, Bairstow FL. 2011 Mapping geomagnetic secular variation at the core–mantle boundary. *Geophysical Journal International* **186**, 521–528. (doi:10.1111/j.1365-246X.2011.05066.x).
- Finlay CC, Jackson A. 2003 Equatorially Dominated Magnetic Field Change at the Surface of Earth's Core. *Science* **300**, 2084–2086. (doi:10.1126/science.1083324).
- Yukutake T. 1962 The Westward Drift of the Magnetic Field of the Earth. *Bulletin of the Earthquake Research Institute - University of Tokyo* **40**, 1–65.
- Jault D, Gire C, Le Mouél JL. 1988 Westward drift, core motions and exchanges of angular momentum between core and mantle. *Nature* **333**, 353–356. (doi:10.1038/333353a0).
- Jackson A. 2003 Intense equatorial flux spots on the surface of the Earth's core. *Nature* **424**, 760–763. (doi:10.1038/nature01879).
- Fisk HW. 1931 Isopors and isoporic movements. In *Terrestrial Magnetism and Electricity of the International Geodetic and Geophysical Union* pp. 280–292. Stockholm.
- Roberts PH, King EM. 2013 On the genesis of the Earth's magnetism. *Reports on Progress in Physics* **76**, 096801. (doi:10.1088/0034-4885/76/9/096801).
- de Wijs GA, Kresse G, Vočadlo L, Dobson D, Alfè D, Gillan MJ, Price GD. 1998 The viscosity of liquid iron at the physical conditions of the Earth's core. *Nature* **392**, 805–807.

- (doi:10.1038/33905).
- 461 12. Proudman J. 1916 On the motion of solids in a liquid possessing vorticity. *Proceedings of*  
462 *the Royal Society of London A: Mathematical, Physical and Engineering Sciences* **92**, 408–424.  
463 (doi:10.1098/rspa.1916.0026).
  - 464 13. Taylor GI. 1917 Motion of solids in fluids when the flow is not irrotational. *Proceedings*  
465 *of the Royal Society of London A: Mathematical, Physical and Engineering Sciences* **93**, 99–113.  
466 (doi:10.1098/rspa.1917.0007).
  - 467 14. Pais MA, Jault D. 2008 Quasi-geostrophic flows responsible for the secular variation of  
468 the Earth's magnetic field. *Geophysical Journal International* **173**, 421–443. (doi:10.1111/j.1365-  
469 246X.2008.03741.x).
  - 470 15. Hide R. 1966 Free Hydromagnetic Oscillations of the Earth's Core and the Theory of the  
471 Geomagnetic Secular Variation. *Philosophical Transactions of the Royal Society of London A:*  
472 *Mathematical, Physical and Engineering Sciences* **259**, 615–647. (doi:10.1098/rsta.1966.0026).
  - 473 16. Finlay CC, Dumberry M, Chulliat A, Pais MA. 2010 Short Timescale Core Dynamics: Theory  
474 and Observations. *Space Science Reviews* **155**, 177–218. (doi:10.1007/s11214-010-9691-6).
  - 475 17. Hori K, Jones CA, Teed RJ. 2015 Slow magnetic Rossby waves in the Earth's core. *Geophysical*  
476 *Research Letters* **42**, 2015GL064733. (doi:10.1002/2015GL064733).
  - 477 18. Hori K, Teed RJ, Jones CA. 2017 The dynamics of magnetic Rossby waves in spherical dynamo  
478 simulations: A signature of strong-field dynamos?. *Physics of the Earth and Planetary Interiors*.  
479 (doi:10.1016/j.pepi.2017.07.008).
  - 480 19. Cardin P, Olson P. 1994 Chaotic thermal convection in a rapidly rotating spherical shell:  
481 consequences for flow in the outer core. *Physics of the Earth and Planetary Interiors* **82**, 235–259.  
482 (doi:10.1016/0031-9201(94)90075-2).
  - 483 20. Schaeffer N, Cardin P. 2005 Quasigeostrophic model of the instabilities of the Stewartson layer  
484 in flat and depth-varying containers. *Physics of Fluids* **17**, 104111. (doi:10.1063/1.2073547).
  - 485 21. Canet E, Finlay CC, Fournier A. 2014 Hydromagnetic quasi-geostrophic modes in  
486 rapidly rotating planetary cores. *Physics of the Earth and Planetary Interiors* **229**, 1–15.  
487 (doi:10.1016/j.pepi.2013.12.006).
  - 488 22. Aubert J, Gillet N, Cardin P. 2003 Quasigeostrophic models of convection in rotating spherical  
489 shells. *Geochemistry, Geophysics, Geosystems* **4**, 1052. (doi:10.1029/2002GC000456).
  - 490 23. Gillet N, Jones CA. 2006 The quasi-geostrophic model for rapidly rotating spherical  
491 convection outside the tangent cylinder. *Journal of Fluid Mechanics* **554**, 343–369.  
492 (doi:10.1017/S0022112006009219).
  - 493 24. Guervilly C, Cardin P. 2016 Subcritical convection of liquid metals in a rotating sphere using  
494 a quasi-geostrophic model. *Journal of Fluid Mechanics* **808**, 61–89. (doi:10.1017/jfm.2016.631).
  - 495 25. Maffei S, Jackson A, Livermore PW. 2017 Characterization of columnar inertial  
496 modes in rapidly rotating spheres and spheroids. *Proc. R. Soc. A* **473**, 20170181.  
497 (doi:10.1098/rspa.2017.0181).
  - 498 26. Jault D. 2008 Axial invariance of rapidly varying diffusionless motions in the Earth's core  
499 interior. *Physics of the Earth and Planetary Interiors* **166**, 67–76. (doi:10.1016/j.pepi.2007.11.001).
  - 500 27. Labbé F, Jault D, Gillet N. 2015 On magnetostrophic inertia-less waves in quasi-geostrophic  
501 models of planetary cores. *Geophysical & Astrophysical Fluid Dynamics* **109**, 587–610.  
502 (doi:10.1080/03091929.2015.1094569).
  - 503 28. Zhang K, Earnshaw P, Liao X, Busse FH. 2001 On inertial waves in a rotating fluid sphere.  
504 *Journal of Fluid Mechanics* **437**, 103–119. (doi:10.1017/S0022112001004049).
  - 505 29. Davidson PA. 2013 *Turbulence in Rotating, Stratified and Electrically Conducting Fluids*.  
506 Cambridge: Cambridge University Press.
  - 507 30. Vallis GK. 2017 *Atmospheric and Oceanic Fluid Dynamics: Fundamentals and Large-Scale*  
508 *Circulation*. Cambridge University Press 2 edition. (doi:10.1017/9781107588417).
  - 509 31. Jault D, Finlay C. 2015 Waves in the core and mechanical core-mantle interactions. In *Treatise*  
510 *on Geophysics* vol. 8 pp. 225–245. Elsevier Science. (doi:10.1016/B978-0-444-53802-4.00150-0).
  - 511 32. Duba CT, McKenzie JF. 2012 Propagation properties of Rossby waves for latitudinal  $\beta$ -plane  
512 variations of  $f$  and zonal variations of the shallow water speed. *Ann. Geophys.* **30**, 849–855.  
513 (doi:10.5194/angeo-30-849-2012).
  - 514 33. Davidson PA, Staplehurst PJ, Dalziel SB. 2006 On the evolution of eddies in a rapidly rotating  
515 system. *Journal of Fluid Mechanics* **557**, 135–144. (doi:10.1017/S0022112006009827).
  - 516 34. Schaeffer N, Jault D, Nataf HC, Fournier A. 2017 Turbulent geodynamo simulations: a leap  
517 towards Earth's core. *Geophysical Journal International* **211**, 1–29. (doi:10.1093/gji/ggx265).

- 518 35. Olson P. 2011 Laboratory Experiments on the Dynamics of the Core. *Physics of the Earth and*  
519 *Planetary Interiors* **187**, 139–156. (doi:10.1016/j.pepi.2011.08.006).
- 520 36. Gillet N, Schaeffer N, Jault D. 2012 Rationale and geophysical evidence for quasi-geostrophic  
521 rapid dynamics within the Earth's outer core. *Physics of the Earth and Planetary Interiors* **202-**  
522 **203**, 78 – 88. (doi:10.1016/j.pepi.2012.03.006).
- 523 37. Abramowitz M, Stegun IA. 1964 *Handbook of Mathematical Functions: With Formulas, Graphs,*  
524 *and Mathematical Tables*. Courier Corporation.
- 525 38. Davidson PA. 2016 Dynamos driven by helical waves: scaling laws for numerical dynamos  
526 and for the planets. *Geophysical Journal International* **207**, 680–690. (doi:10.1093/gji/ggw297).
- 527 39. Roberts PH, Scott S. 1965 On analysis of the secular variation. *Journal of geomagnetism and*  
528 *geoelectricity* **17**, 137–151.
- 529 40. Finlay C. 2005 *Hydromagnetic waves in Earth's core and their influence on geomagnetic secular*  
530 *variation*. PhD thesis The University of Leeds.
- 531 41. Aubert J, Finlay CC, Fournier A. 2013 Bottom-up control of geomagnetic secular variation by  
532 the Earth's inner core. *Nature* **502**, 219–223. (doi:10.1038/nature12574).
- 533 42. Hide R, Roberts PH. 1979 How strong is the magnetic field in the Earth's liquid core?. *Physics*  
534 *of the Earth and Planetary Interiors* **20**, 124–126. (doi:10.1016/0031-9201(79)90034-7).